Acta Materialia 176 (2019) 211–219

Contents lists available at ScienceDirect

Acta Materialia

journal homepage: www.elsevier.com/locate/actamat

Full length article

Twinning stress of type I and type II deformation twins

Peter Müllner

Micron School of Materials Science and Engineering, Boise State University, Boise, ID 83725, USA

ARTICLE INFO

Article history:
Received 25 March 2019
Received in revised form
1 July 2019
Accepted 2 July 2019
Available online 4 July 2019

Keywords:
Twin boundary mobility
Shape memory alloy
Topological model
Dislocation
Disconnection

ABSTRACT

Recent reports on highly mobile type II twin boundaries challenge the established understanding of deformation twinning and motivate this study. We consider the motion of twin boundaries through the nucleation and growth of disconnection loops and develop a mechanism-based model for twin boundary motion in the framework of isotropic linear elasticity. While such mechanisms are well established for type I and compound twins, we demonstrate based on the elastic properties of crystals that type II twin boundaries propagate in a similar way. Nucleation of a type I twinning disconnection loop occurs in a discrete manner. In contrast, nucleation of a type II twinning disconnection loop occurs gradually with increasing Burgers vector. The gradual nucleation of a type II disconnection loop accounts for the higher mobility of type II twin boundaries compared with type I twin boundaries. We consider the homogeneous nucleation of a disconnection loop, which is adequate for twinning in shape memory alloys with a low-symmetry crystal lattice. For the magnetic shape memory alloy Ni–Mn-Ga, the model predicts twinning stresses of 0.33 MPa for type II twinning and 4.7 MPa for type I twinning. Over a wide temperature range, the twinning stress depends on temperature only through the temperature dependence of the elastic constants, in agreement with experimental results.

1. Introduction

In 2011, Straka et al. reported twinning stresses of 1.2 MPa and 0.05 MPa for type I and type II twins for the same Ni–Mn-Ga single crystal sample [1]. These values are twofold extraordinary. First, 0.05 MPa is probably the lowest yield stress measured for any metal so far. Second, the ratio of type I and type II twinning stresses is 24. Considering that the shear strains for type I and type II twins are identical [2] and the shear stiffness on the two shear systems is almost identical, such a large ratio requires an explanation. In this article, we develop a twinning model based on isotropic linear elastic dislocation theory that provides answers to why the twinning stress is so low and why it is different for type I and type II twins.

Twinning is a major mode of plastic deformation for example in hexagonal close-packed metals [2] and nano-crystalline and nano-structured face-centered cubic metals [3–5]. In addition, twinning in functional materials such as shape memory alloys [6], ferroelastic minerals [7], and ferroelectric ceramics [8], is associated with a significant strain and provides the mechanisms for transformation between electric/magnetic/thermal energy and mechanical energy.

Structural and functional materials represent two extremes regarding their requirement on twin boundary mobility. For structural materials on the one hand, the twinning stress must be high to provide strength to the material. For example, in twin-induced plasticity (TWIP) steel, the twinning stress after grain refining and work-hardening exceeds 1.7 GPa [9,10]. For functional materials, the twinning stress must be low to reduce mechanical losses associated with the conversion from mechanical to electrical energy and vice versa. The stress values are very small indeed as mentioned at the beginning of this introduction at the example of Ni-Mn-Ga [1,11].

The high twinning stress in structural materials results from a relatively large twinning shear and associated large Burgers vector of twinning disconnections. Many twinning mechanisms were described in the literature for such materials and Christian and Mahajan presented a comprehensive review [2]. The high mobility of twin boundaries in functional materials results from the small twinning shear and associated small Burgers vector of twinning disconnections. In materials with a shear instability such as many martensites [12] the low shear stiffness on the twinning system further reduces the twinning stress. Existing models rationalize the variation of twin boundary mobility and twinning stress due to variations of material parameters such as shear modulus and lattice parameter. Such models explain why different materials have

E-mail address: petermullner@boisestate.edu.

https://doi.org/10.1016/j.actamat.2019.07.004
1359-6454/

different twin boundary motility and twinning stress (e.g. Refs. [13,14]).

Models that relate the twinning stress solely to the shear modulus and twinning shear cannot account for the differences in twinning stress of type I and type II twins. Straka et al. reported 0.05 and 1.2 MPa twinning stress for type II and type I twins [1]. Similarly, Kellis et al. [15] reported for one sample magnetic switching fields of 30 and 300 mT where the higher value was associated with type I twins and the lower value with type II twins. Saren et al. [16] and Smith et al. [17] reported a boundary velocity of 39 and 82 m/s for type II twins in 10 M Ni–Mn-Ga. Faran and Shilo studied the kinetics of twin boundaries and reported that at a driving force of 100 kJ/m^3 type II twin boundaries move ten times faster than type I twin boundaries [18]. 10 M Ni–Mn-Ga is almost tetragonal such that the shear stiffness for type I and type II twinning is almost identical. The shear is the same for both twin types. Thus, current mechanism-based models do not account for the one order of magnitude difference of twin boundary mobility of type I and type II twins.

Here we present twin boundary propagation models for type I and type II twins and derive the twinning stress and its temperature dependence. We assume that the nucleation of a twinning disconnection loop controls the twinning stress. We obtain the twinning stress from comparing the energy of the growing disconnection loop with the work done by the stress when expanding the loop. We build on the topological model of interfaces [19,20]. In section 2, we evaluate the assumptions implied in the model. In section 3, we treat straight twinning disconnections to establish their Burgers vector and step height. For type I twins, this approach is well established. We show that this concept also applies to type II twin boundaries. In section 4, we consider the nucleation of a circular disconnection loop and derive the twinning stress. In section 5, we calculate the activation energy of twin nucleation. In section 6, we first discuss the implications of the model for general shear band deformation and then apply it to twinning in 10 M Ni–Mn-Ga.

2. Methodology

We relate mechanical properties to the microscopic mechanism of deformation twinning. This is a classical task of physical metallurgy. The incommensurate nature of type II twin boundaries (with an irrational $\mathbf{K}_1$ plane) presents challenges to a rigorous treatment. Atomistic simulations require a prohibiting large computer power to address the problem. Geometrical models relying on periodicity fail at the non-periodic structure, too. The topological model falls into this latter category. It is an extension of crystallography to bicrystals. It deals with geometry alone and disregards interatomic forces. In particular, the topological model correlates crystal structure, bicrystal misorientation, and interface defects. The topological model cannot predict the particular atomic structure of an incommensurate interface. However, it does predict the defect content of an interface. We take results from the topological model and apply linear, isotropic elasticity to derive energies and stresses associated with interfacial defects. In this section, we discuss the assumptions of our method and their implications.

2.1. Linear elasticity

Linear elasticity fails at sub-atom length scale. Linear elasticity does not accurately describe stresses near the dislocation line. To account for this limitation, scientists introduced an inner cut-off radius ρ to delineate the dislocation core (within which linear elasticity fails) from the bulk material for which linear elasticity appropriately describes elastic fields. In section 4.1, we derive the critical radius for nucleation of a type I disconnection loop, which is five times the inner cut-off radius for a dislocation (Equation (13)). Thus, the calculations are within the validity regime of linear elasticity, albeit close to its lower limit. We conclude that applying linear elasticity is reasonable though it may overestimate the energy of a dislocation loop. Therefore, linear elasticity overestimates the twinning stress somewhat.

2.2. Isotropic elasticity

Isotropic elasticity assumes that the shear stiffness is the same for all shear systems. Shape memory alloys have low crystal symmetry and the shape memory effect and twinning relate to a martensitic transformation. Thus, shape memory alloys are inherently elastically anisotropic materials and isotropic elasticity does not accurately predict mechanical properties. Here we assess how anisotropy impacts the results obtained in section 4. In many materials undergoing a martensite transformation, the shear stiffness for twinning relates to the C' modulus of the austenite phase [12]. These materials typically exhibit a softening of the TA_2 phonon branch which weakens the C' modulus. C' is substantially lower than the shear stiffness on other shear systems. In particular, C' is substantially lower than the shear modulus G of an isotropic material, for which $G = Y/(1+\nu)$, where Y is the Young modulus and ν is the Poisson ratio. The strain energy density ε is obtained from the stress tensor σ_{ij} and strain tensor ε_{kl}:

$$\varepsilon = \frac{1}{2}\sigma_{ij}\varepsilon_{kl} = \frac{1}{2}c_{ijkl}\varepsilon_{kl}^2 \tag{1}$$

where the non-vanishing stiffness components c_{ijkl} are typically larger than the soft C'. Estimating the strain energy through C' (Equation (10)) therefore underestimates the loop energy and, thus, the twinning stress.

2.3. Discrete disconnection core

The core of a disconnection may spread over a certain distance. Spreading reduces the core energy. We treat the twinning disconnections as having a narrow, discrete core. Therefore, by assuming a discrete disconnection core, we overestimate the disconnection energy, and, thus, the twinning stress.

2.4. Implications

The relative strength of the errors made by assuming linear elasticity, isotropy, and discrete disconnection core are difficult to assess. Further, the models include various parameters for which exact numerical values may not be available. Therefore, numerical results presented in section 6 may be off by a sizable factor of 2 or even more. However, the errors are systematical. For example, the twinning stresses for type I and type II twinning are proportional to the shear modulus G (Equations (14) and (19)). We conclude that the errors made by the simplifications are similar for both twinning types. Therefore, the presented models allow (i) a qualitative comparison of type I and type II twinning stresses, (ii) the prediction of the dependences of twinning stress and activation energy on material properties such as elastic constants and lattice parameters, and (iii) a qualitative assessment of the temperature dependence of the twinning stress. We limit the discussion of the results to such a comparative assessment. We learn from this analysis what similarities exist between type I and type II twinning and some fundamental differences. An exact quantitative prediction of twinning stresses is beyond the scope of this study.

3. Twin boundary propagation

Following the topological model (TM) introduced by Hirth and Pond [19], crystalline interfaces move through the propagation of disconnections along the interface. A disconnection is a line defect located in the interface and containing dislocation character (with Burgers vector **b**) and step character (with step height h). The disconnection line separates planar and parallel interface terraces. As the disconnection moves, the dislocation component generates deformation while the step component transforms a volume increment from belonging to the one side of the boundary to belonging to the other side.

In the case of deformation twinning, the Burgers vector is parallel to the twinning direction and the step height is the ratio of the magnitude b of the Burgers vector and the twinning shear s:

$$h = \frac{b}{s} \tag{2}$$

Throughout section 3, we consider straight dislocations, disconnections, and disclinations. We consider approximations for small twinning shear $s \ll 1$ such that $\cos(s) = 1, \sin(s) = \tan(s) = s$, and due to the symmetry of the stress state the shear stresses on the primary and conjugate twinning systems are identical.

3.1. Type I twins

Vladimirsky [21] and Frank and van der Merwe [22] introduced the twinning dislocation (Fig. 1a) as the elementary carrier of deformation for a moving twin boundary. The twinning dislocation makes intuitively sense for type I twins (and also for compound twins) because the twinning plane $\mathbf{K}_1$ is rational. The step height h_I is the d-spacing $d_{\mathbf{K}_1}$ of the twinning plane and the Burgers vector b_I is (Fig. 1b):

$$b_\mathrm{I} = s d_{\mathbf{K}_1} = s h_\mathrm{I} \tag{3}$$

The work w_I per line length (unit J/m) done by a stress when moving the twinning dislocation is the Peach-Koehler force $F_\mathrm{PK} = \tau b$ multiplied by the distance Δx travelled by the dislocation:

$$w_\mathrm{I} = \tau b_\mathrm{I} \Delta x = \tau h_\mathrm{I} s \Delta x \tag{4}$$

Scientists established the twinning dislocation through many quantitative studies using transmission electron microscopy. The terms twinning dislocation and twinning disconnection are exchangeable. Here we favor the term twinning disconnection since this term highlights the presence of a step which plays a critical role in establishing the twinning stress.

3.2. Type II twins

Bullough suggested a dislocation mechanism for twinning where shear occurs on the conjugate twinning plane [23]. Cahn [24] and Hirth and Lothe [25] interpreted this mechanism in terms of conjugate dislocations moving on conjugate twinning planes. Pond and Hirth advanced a quantitative topological model for type II twinning akin to Bullough's concept and applied it with high accuracy to type II twinning in alpha uranium [26] and NiTi [27]. Following the topological model for type II twins, the twin boundary contains a wall of dislocations with Burgers vector $\mathbf{b}_\mathrm{ct}$ perpendicular to the boundary plane (Fig. 2a). The relationship between the magnitude b_ct of $\mathbf{b}_\mathrm{ct}$, the d-spacing $d_{\mathbf{K}_2}$ of conjugate twinning planes, and the primary (i.e. type I) twinning dislocation is [2]:

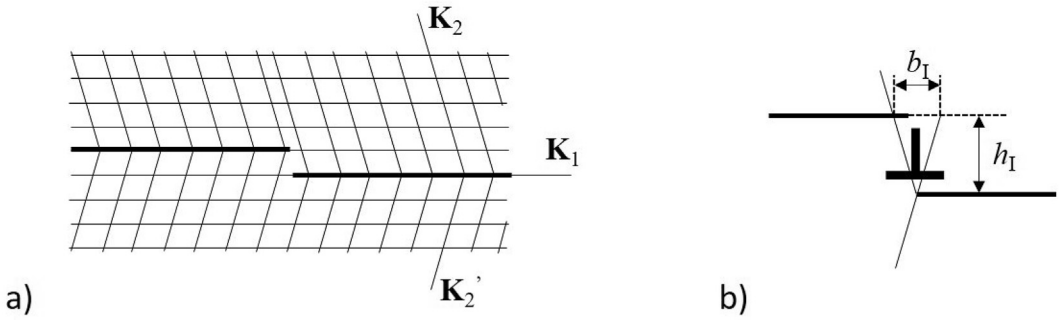

Fig. 1. A twinning disconnection; (a) a step in the twin boundary generates a displacement field which is illustrated schematically as a compression of $\mathbf{K}_2$ planes in the upper half-crystal; (b) The twinning planes $\mathbf{K}_1$ and $\mathbf{K}_2$ define Burgers vector and step height.

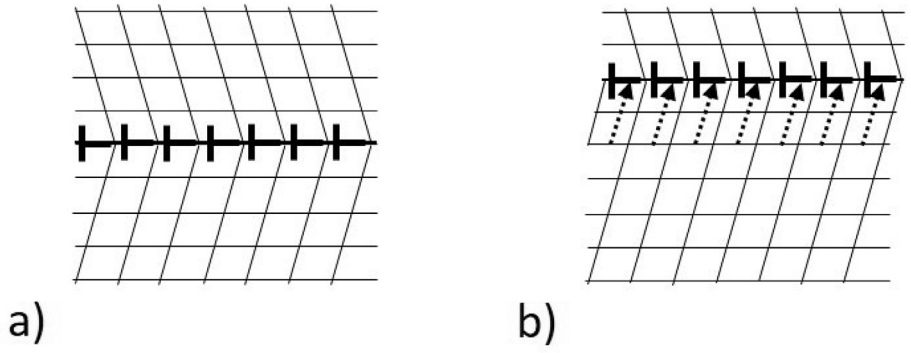

Fig. 2. Dislocation model of a type II twin boundary; (a) conjugate dislocations line up in the twin boundary such that their Burgers vector is perpendicular to the twin boundary; (b) the twin boundary moves when all conjugate dislocations move collectively.

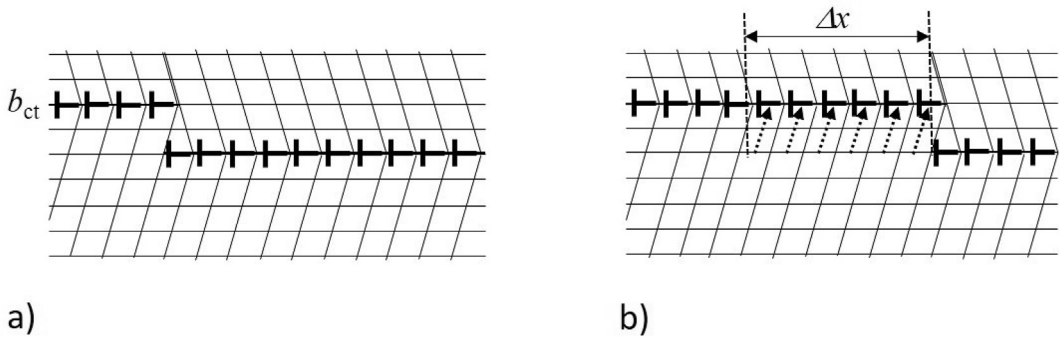

Fig. 3. Discrete motion of a type II twin boundary following the topological model [25]; (a) a step in a type II twin boundary is a disconnection similar to that shown in Fig. 1 with Burgers vector and step height; the displacement field is schematically illustrated by the compressed $\mathbf{K}_2$ planes in the upper half-crystal; (b) the twinning disconnection moves to the right when successive conjugate dislocations move from the lower terrace position to the upper terrace position.

$$s = \frac{b_{\mathrm{I}}}{d_{\mathbf{K}_1}} = \frac{b_{\mathrm{ct}}}{d_{\mathbf{K}_2}} \tag{5}$$

A type II twin then grows by the collective motion of these conjugate dislocations (Fig. 2b). As the dislocations move, the top half-crystal shifts by a displacement $\Delta u = s\Delta y$ where Δy is the distance travelled by the twin boundary. Therefore, the net motion of the dislocation is parallel to the transformed conjugate twinning plane. The Burgers vector $\mathbf{b}_{\mathrm{ct}}$ of the conjugate twinning dislocations is perpendicular to the twin boundary because the twinning shear on the primary twinning plane is the superposition of a simple shear on the conjugate system and a rotation. This rotation is partitioned between both half-crystals [25–29] such that the conjugate dislocations end up perpendicular to the interface.

The twin boundary is in mechanical equilibrium when it is flat and parallel to $\mathbf{K}_1$. Thus, a twin boundary stays in mechanical equilibrium if it moves rigidly with all twinning dislocations moving synchronously as shown in Fig. 2b. However, moving a planar boundary rigidly requires the simultaneous braking of all bonds on the interface. This requires a high energy and, thus, a high stress. It requires less stress to move a dislocation on its glide plane than to rigidly move a crystal on a slip plane. Analogously, it requires less stress to move a step along a type II twin boundary compared to moving the type II twin boundary rigidly. We further expand this argument in section 4.2.

Fig. 3 illustrates the motion of a step in a type II twin boundary. On either side of the step, the twin boundary consists of a semi-infinite wall of dislocations. For the step to move a distances Δx along the twin boundary, N dislocations move from one boundary level by the step height to the next boundary level such that $\Delta x = Nd_{\mathbf{K}_2}$. The work w_{IIct} done by a stress on the moving dislocations is the Peach-Koehler force $F_{\mathrm{PK}} = \tau b$ multiplied by the number of dislocations and the distance h_{II} travelled by the dislocations where h_{II} is the step height (with the approximation for small shear mentioned earlier):

$$w_{\mathrm{IIct}} = N\tau b_{\mathrm{ct}} h_{\mathrm{II}} = \tau h_{\mathrm{II}} s\Delta x \tag{6}$$

The step in the twin boundary can be interpreted by dislocations $\mathbf{b}_{\mathrm{ct}}$ as shown in Fig. 4a. Alternatively, each semi-infinite wall of dislocations can be represented by a disclination with strength $\omega_{1,2} = \pm s$ ([30,31], Fig. 4b). The two disclinations form a disclination dipole, which has a dislocation equivalent with Burgers vector $\mathbf{b}_{\mathrm{II}}$ perpendicular to the line direction of the disclinations and perpendicular to the plane containing both disclinations (Fig. 4c). The magnitude b_{II} of $\mathbf{b}_{\mathrm{II}}$ is:

$$b_{\mathrm{II}} = h_{\mathrm{II}}\omega = h_{\mathrm{II}} s \tag{7}$$

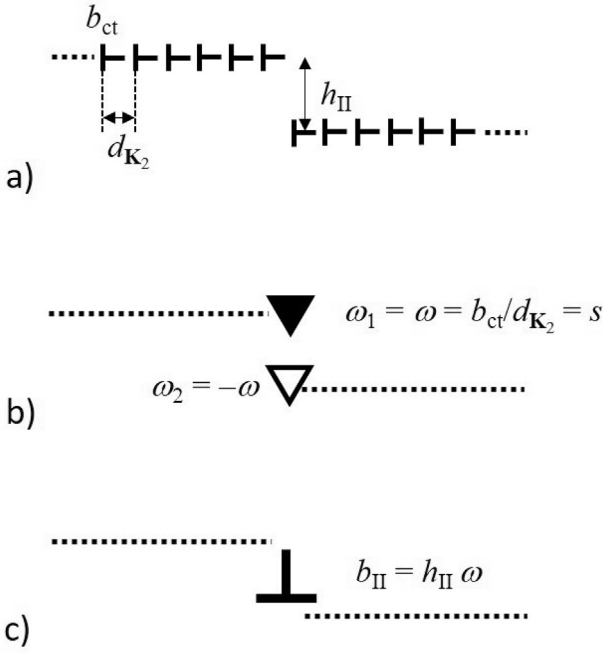

Fig. 4. Displacement field of a type II twinning disconnection; (a) the displacement field of the disconnection is the sum of the displacement fields of all conjugate dislocations; (b) on each terrace, the semi-infinite walls of conjugate dislocations form a disclination; the displacement field of the disconnection is the sum of the displacement fields of two disclinations with strength $\omega_{1,2} = \pm s$ (i.e. the displacement field of a disclination dipole); (c) a disclination dipole can be approximated by a single dislocation with a Burgers vector perpendicular to the direction of the disclination lines; the displacement field of the disconnection is that of a dislocation with Burgers vector $b_{\mathrm{II}} = sh_{\mathrm{II}}$.

All three defect representations shown in Fig. 4a–c have the same displacement, strain, and stress fields (except within a boundary layer with thickness equal to the distance $d_{\mathbf{K}_2}$). Thus, the step in the type II interface is a disconnection with Burgers vector $\mathbf{b}_{\mathrm{II}}$ and step height h_{II}. The work w_{II} done by a shear stress when moving the disconnection by Δx is:

$$w_{\mathrm{II}} = \tau b_{\mathrm{II}}\Delta x = \tau h_{\mathrm{II}} s\Delta x \tag{8}$$

3.3. Conclusions from considering straight twinning disconnections

We have shown that for type I and type II twins the propagation of the twin boundary occurs through the motion of disconnections.

The motion of the type II twinning disconnection can be viewed as resulting from the collective motion of conjugate twinning dislocations. Comparison of Equations (6) and (8) shows that the two interpretations are indeed equivalent. For type I and type II twinning, the work per line length done by a stress when moving a twinning disconnection equals the product of stress, step height, twinning shear, and distance travelled.

4. Nucleation of a disconnection loop

The lateral growth of a twin requires the nucleation of twinning disconnections. The nucleation of a disconnection is a three-dimensional process and cannot be modeled by straight dislocations. In this section, we consider circular disconnection loops represented by a dislocation glide loop (or briefly a glide loop).

The nucleation of the glide loop requires a shear stress. When the glide loop grows, the shear stress does work, which is proportional to the shear stress, the Burgers vector, and the area swept by the glide loop:

$$W_\mathrm{L} = \pi\tau b_\mathrm{I} R^2 \tag{9}$$

We denote the work with a capital W to indicate that this is an absolute work (with unit J), and not a work per line length as in Equations (4), (6) and (8).

From the first law of thermodynamics follows that the work done by the stress when growing the glide loop must be equal or larger than the energy E of the glide loop [32]:

$$E = \frac{(2-\nu)}{4(1-\nu)} GRb^2 \left(ln\frac{4R}{\rho} - 2 \right) \tag{10}$$

where ν and ρ are the Poisson ratio and the inner cut-off radius (measured from the disconnection line) below which linear elasticity theory fails. The shear stress required to grow the glide loop infinitely is the twinning shear stress.

4.1. Type I twins

For a type I twin, the step height is constant $h_\mathrm{I} = d_{K_1}$ and, thus, the Burgers vector is constant (Equation (3)). Comparing equations (9) and (10) we notice that at small R the work increases more slowly than the loop energy. In contrast at large R, the work increases faster than the loop energy. For low stress values, the Energy of the loop exceeds the work for a wide range of R (Fig. 5). With increasing stress, that range decreases. At the critical stress (i.e. the twinning stress τ_I) this range vanishes, and $E(R)$ and $W_\mathrm{L}(R)$ have one common point with a common tangent:

$$E(R) = W_\mathrm{L}(R, \tau_\mathrm{I}) \tag{11}$$

$$\frac{dE(R)}{dR} = \frac{dW_\mathrm{L}(R, \tau_\mathrm{I})}{dR} \tag{12}$$

which yields the critical radius R_cI:

$$R_\mathrm{cI} = \frac{e^3}{4}\rho \cong 5\rho \tag{13}$$

and the twinning stress τ_I:

$$\tau_\mathrm{I} = \frac{(2-\nu)Gb_\mathrm{I}}{\pi(1-\nu)e^3\rho} \tag{14}$$

At stresses larger than τ_I, the work done by the growing loop is always greater than the energy of the loop. We therefore take τ_I as the twinning stress for type I twins. At a radius larger than R_cI, the glide loop grows stably at a stress less than τ_I.

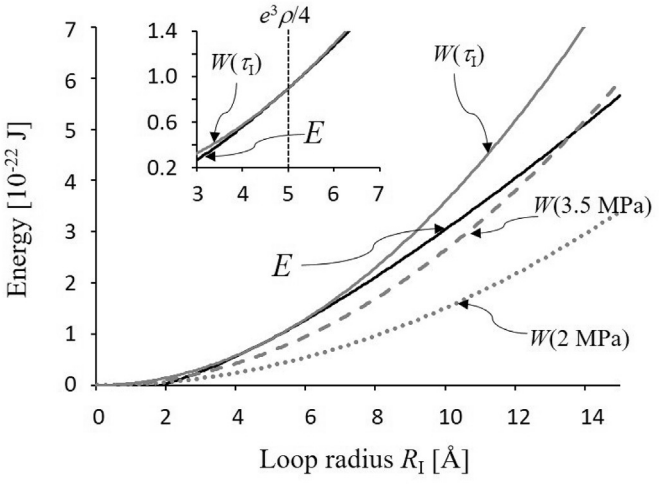

Fig. 5. Loop energy and work done by a growing type I disconnection loop with $G = 0.5$ GPa, $\nu = 1/3$, $s = 0.12$, $h = 2$ Å and $\rho = 1$ Å (Table 1); the black solid line represents the loop energy, the gray lines represent the work done by a stress of 2 (dotted) and 3.5 MPa (dashed) and by the critical stress τ_I (solid). For low stress, the work increases more slowly at small loop radius than the loop energy. With increasing radius, the work increases more steeply and eventually equals the work. With increasing stress, the region where the loop energy exceeds the work decreases. At τ_I, the work equals or exceeds the loop energy for all radii. Thus, τ_I defines the twinning stress. The inset shows that the work and the loop energy have a common point with common tangent at $R_\mathrm{I} = R_\mathrm{cI} = \frac{e^3}{4}\rho$ and $\tau = \tau_\mathrm{I}$.

4.2. Type II twins

For a type II twin with an irrational twinning plane, crystallography does not define the step height of the disconnection. Further, one may argue that type II twin boundaries move without steps because their energy does not depend on the boundary position. In section 4.2, we first show that this argument is incorrect. We then identify what is a reasonable step height for a type II disconnection. Finally, we develop a nucleation model for a disconnection loop that derives from the variability of the step height.

The elasticity of the interface introduces a threshold on boundary movement. The argumentation is similar to that presented by Fleischer for solid solution hardening [33,34]: Considering a straight and rigid dislocation moving on its glide plane through a crystal with a random distribution of solute atoms, the average interaction force of the stress fields of the solute atoms on the dislocation is zero. One might erroneously conclude that solute atoms do not increase the yield strength. However, the assumption of a *rigidly straight* dislocation is not correct. At any given average position of the dislocation, the dislocation reacts to the local stress field of the nearest solute atoms. Dislocation segments find local energy minima, *i.e.* the dislocation line is not exactly straight but meanders about a straight line. When the dislocation moves, a force is required to pull the dislocation segments out of their local energy minima. Thus, the elasticity of the dislocation line results in a net retracting force that is solid solution strengthening.

Similarly, we may consider the rigid propagation of a twin boundary. If a type II twin boundary with an irrational twinning plane moved such that the adjacent crystals are absolutely rigid, the overall structure of the twin boundary remains identical. In such a case, the energy of the interface did not depend on the boundary position and the boundary moved without hindrance, i.e. the twinning stress was zero. However, the assumption of

absolutely rigid crystals is incorrect. The atoms adjacent to the twin boundary relax to find local energy minima. Applying density functional theory, Wang and Sehitoglu calculate the value of the displacements of atoms at twin boundaries of shape memory alloys [14]. They obtained maximum displacements "within 1% of the Burgers vector". When the boundary moves, each atom has to be pushed out of a local energy minimum. This requires a force.

We model this force by assuming elastic interaction between the atoms. Moving the boundary locally away from its equilibrium position creates a strained state within the volume swept by the boundary with the local strain energy density ε_λ:

$$\varepsilon_\lambda = \frac{1}{2}\sigma_{ij}\varepsilon_{kl} \approx \tau_\lambda \gamma_\lambda = G\gamma_\lambda^2 \tag{15}$$

where γ_λ is the strain produced by the local relaxation displacement and τ_λ is the stress resulting from restoring that displacement. The strain energy density increases with increasing distance from the equilibrium position of the boundary until, at a critical distance h_c, the atoms break away from their local energy minima.

Fig. 6 illustrates the formation of a type II disconnection loop. The figure is drawn in two versions: on the left side in two dimensions using straight dislocations and disconnections and on the right side in three dimension with disconnection loops. A disconnection dipole (2D) or loop (3D) may form through a gentle undulation of the twin boundary (Fig. 6a) that growths into a stable loop. We approximate the undulation (which we call nascent loop) with a rectangular profile and a circular loop of small step height (Fig. 6b). The nascent loop may grow by increasing the step height and by increasing the radius. We assume that the nascent loop first grows with constant radius R_{nII} and increasing step height h_{nII} (Fig. 6c) and later transitions into lateral growth (i.e. increasing radius) with constant step height (Fig. 6d). In the first stage, the energy of the nascent loop has two contributions. The first contribution is the line energy E_D of the disconnection. The Burgers vector increases linearly with the step height and, thus, the first energy contribution is quadratic in the step height h_{nII}. The second contribution is the energy E_α required to pull the atoms away from their local energy minima (Equation (15)), which is linear in h_{nII}:

$$E_{\mathrm{nII}} = E_D + E_\alpha = \frac{(2-\nu)}{4(1-\nu)} G R_{\mathrm{nII}} s^2 h_{\mathrm{nII}}^2 \left(ln \frac{4R_{\mathrm{nII}}}{\rho} - 2 \right) + \pi R_{\mathrm{nII}}^2 \varepsilon_\alpha h_{\mathrm{nII}} \tag{16}$$

For the nascent loop, the work W_{nII} is proportional to the transformed volume and increases linearly with the growth:

$$W_{\mathrm{nII}} = \pi R_{\mathrm{nII}}^2 \tau s h_{\mathrm{nII}} \tag{17}$$

The energy has a quadratic term in the step height and eventually exceeds the work with increasing step height. When the energy equals the work, the nascent loop can no longer increase in height. Following results in Ref. [14], the maximum displacement in the twin boundary (resulting from relaxation) is approximately αr_0 where r_0 is an atomic length equivalent to the type I Burgers vector, where α is a dimensionless relaxation parameter in the order of 0.01. At this distance h_c, the local energy density vanishes. Thus, h_c marks the step heights at which the disconnection nucleus can transition from thickness growth (with increasing Burgers vector) to lateral growth (with constant burgers vector):

$$h_c = \frac{\alpha r_0}{s} \tag{18}$$

At the transition, $\gamma_\lambda = \alpha s$, and we obtain the type II twinning stress τ_{II} from $E_{\mathrm{nII}} = W_{\mathrm{nII}}$ with $h_{\mathrm{nII}} = h_c = h_{\mathrm{II}}$:

$$\tau_{\mathrm{II}} = G\alpha^2 s + \frac{(2-\nu)}{\pi(1-\nu)} G\alpha \frac{r_0}{4R_{\mathrm{nII}}} \left(ln \frac{4R_{\mathrm{nII}}}{\rho} - 2 \right) \tag{19}$$

Fig. 7 displays the loop energy E_{nII}, and its two contributions E_D and E_α, and the work W for a stress of 0.2 MPa (gray dotted) and for the twinning stress τ_{II} (gray solid) as a function of step height. The slope of $W_{\mathrm{nII}}(h)$ is proportional to the stress. At low stress, $W_{\mathrm{nII}}(h)$ intersects $E_{\mathrm{nII}}(h)$ below h_c, which prevents the transition to lateral growth. At $\tau = \tau_{\mathrm{II}}$ (gray solid line), the work intersects the total energy at $h = h_c$. At the stress τ_{II}, the work is sufficient to enable the transition to lateral growth.

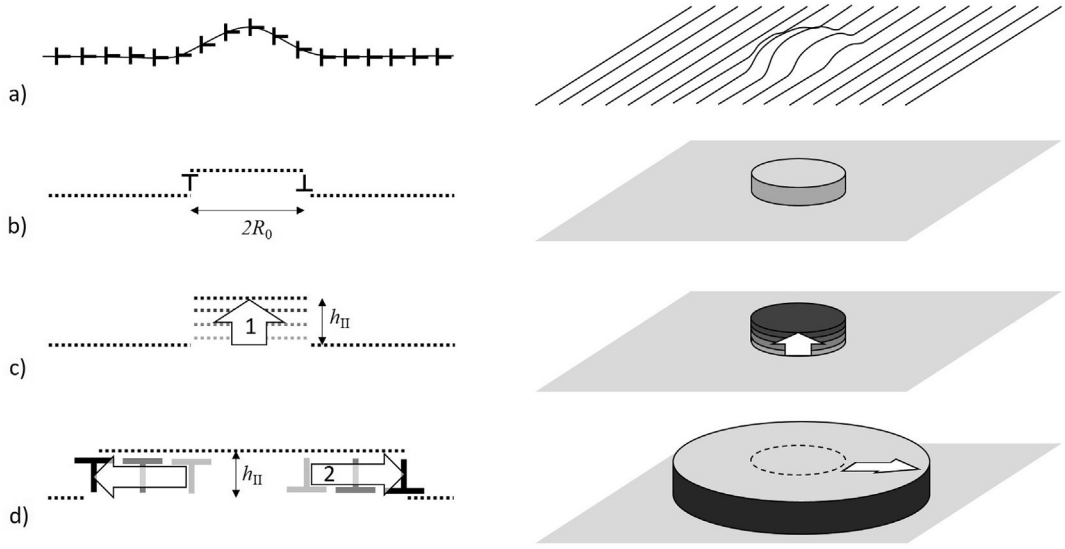

Fig. 6. Formation of a disconnection loop in a type II twin boundary in a two-dimensional schematic (left) and three-dimensional representation (right); (a) The displacement (2D, left) or bowing (3D, right) of a few dislocations creates a twin boundary undulation; (b) a disconnection pair (2D, left) or loop (3D, right) represents the nascent disconnection loop; (c) in stage one of the loop nucleation, the nascent disconnection loop grows by increasing its step height h_{II}; (d) in stage two, the step height remains constant and the disconnection loop grows by increasing its radius.

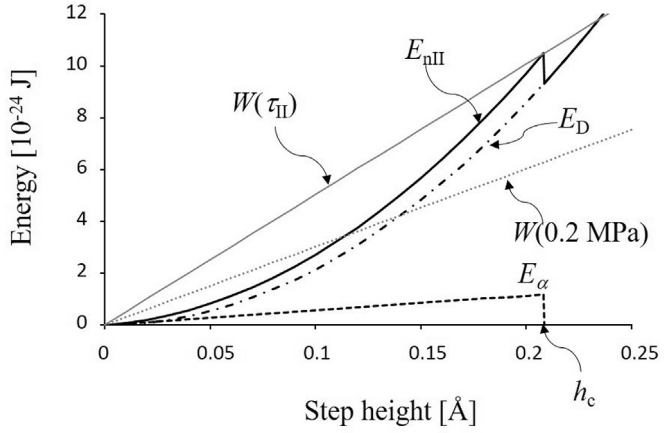

Fig. 7. Loop energy and work done by a nascent type II disconnection loop with $G = 0.5$ GPa, $\nu = 1/3$, $s = 0.12$, and $\rho = 1$ Å (Table 1); the black dash-dotted, dashed, and solid lines represent the loop line energy, the energy required to break atoms away from their local equilibrium site, and the total energy (Equation (16)). The gray lines represent the work done by growing the nascent loop at 0.2 MP (dotted) and at the twinning stress τ_{II} (solid). The work at τ_{II} intersects the total energy at $h = h_c$ and is sufficient to trigger the transition from thickness growth to lateral growth.

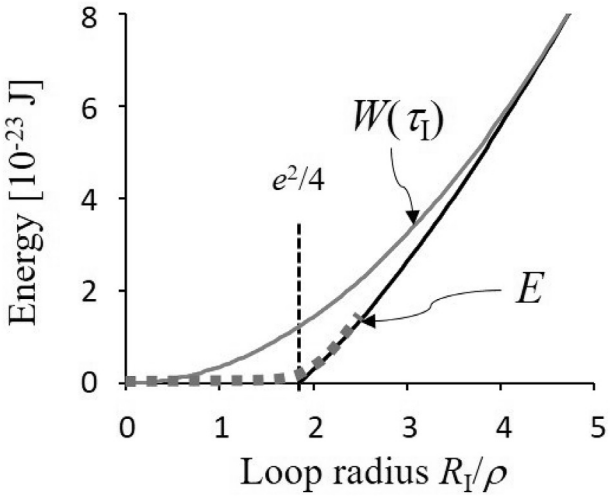

Fig. 8. Loop energy (Equation (9), black solid line) and work done by the twinning stress τ_I (Equation (8), grey solid line) for small loop radii; below $R/\rho = e^2/4$, Equation (9) fails at representing the loop energy, which may be approximated by the dotted grey line. The Orowan stress (Equation (19)) is largest at $R/\rho = e^2/4$.

5. Thermal activation

A process is thermally activated if the thermal energy kT is less than the activation energy E_A. At temperatures above the critical temperature $T_c = E_A/k$, the process is athermal. This does not mean that the twinning stress vanishes. Also, the twinning stress may depend on temperature above T_c. At temperatures $T > T_c$ every attempt to form a disconnection loop is successful. This is not the case below T_c. In this section, we find the activation energy for type I and type II twinning. From Equations (14) and (19) follows that at temperatures higher than T_c, the twinning stress depends on temperature through the temperature dependences of the shear modulus and of the twinning shear, i.e. the lattice parameters.

5.1. Type I twinning

The Orowan stress τ_{OR} is the stress required to keep a glide loop stable against its tendency to shrink to reduce its strain energy (Equation (10)). The Orowan stress is the derivative of the loop energy with respect to radius divided by Burgers vector and loop circumference.

$$\tau_{OR} = \frac{1}{2\pi R b}\frac{dE(R)}{dR} \tag{20}$$

At $R = R_{cI}$, the Orowan stress equals the twinning stress, $\tau_{OR} = \tau_I$. For smaller radii, $R < R_{cI}$, the Orowan stress exceeds the twinning stress. In this regime, the disconnection loop is unstable under the twinning stress and collapses spontaneously. To grow a loop at the twinning stress to the critical radius R_{cI} requires thermal activation.

To estimate the activation energy, we find an upper limit for the Orowan stress. Thermal activation must provide the additional work done by the Orowan stress above the work done by the twinning stress when growing the loop to R_{cI}. In other words, the activation energy is the difference between the work done by the Orowan stress and the work done by the twinning stress (Equation (9)). Fig. 8 shows the work done by the twinning stress and the loop energy for small radii. According to Equation (10), below $R = R_0 = e^2\rho/4$, the loop energy is negative, which is unreasonable and indicates that linear elasticity fails below R_0. The grey dotted line in Fig. 8 marks a more realistic path of the $E(R)$ for very small R.

We can take the Orowan stress at R_0 as an upper limit for the highest Orowan stress occurring during growth of the loop nucleus and find an upper limit for the activation energy E_{AI}:

$$E_{AI} \le (\tau_{OR}(R_0) - \tau_I)\pi b_I R_{cI}^2 = \frac{(2-\nu)(e-2)Gb_I^2 e^3 \rho}{32(1-\nu)} \tag{21}$$

This limit of the activation energy depends only on material parameters including elastic constants (G, ν, ρ) and the Burgers vector.

5.2. Type II twinning

Similar to the Orowan stress, we may define a stress that is required to stabilize the loop against collapsing by reducing the step height. We call this stress step stress. In an area below h_c, the work done by the slope of the energy is larger than the slope of the work done by the twinning stress (Fig. 7). Therefore, the work done by the twinning stress is smaller than the work done by the step stress. The step stress has a maximum at $h = h_c$. Similar to the case of type I twinning, we find an upper limit for the activation energy E_{AII} in the difference of the work done by the step stress and the work done by the twinning stress when increasing the step height under constant stress τ_{II} up to $h = h_c$:

$$E_{AII} \le \left(\frac{dE_{AII}}{dh} - \frac{dW}{dh}\right)h_c = \frac{(2-\nu)}{(1-\nu)}G\alpha^2 r_0^2 R_{nII}\left(ln\frac{4R_{nII}}{\rho} - 2\right) \tag{22}$$

The activation energy E_{AII} contains the radius R_{nII} which is not an intrinsic material parameter. R_{nII} depends on the local atomic arrangement and varies with position since the interface plane is irrational. A smaller radius leads to a smaller activation energy (Equation (22)) but a higher twinning stress (Equation (19)).

6. Discussion

6.1. Discontinuous versus continuous twin boundary motion

We derive the twinning stress for type I and type II twins starting with the assumption that a twin boundary moves through the nucleation and growth of a disconnection loop (i.e. an interface terrace). While such mechanisms are well established for type I and

compound twins, this is not the case for type II twins. We argue that if a boundary moved continuously as a planar defect without disconnections, such a mechanism would require a high stress. We attribute this stress to the local relaxation of atoms at the interface. This effect is stronger the more compliant the lattice is because the relaxation parameter α increases with decreasing stiffness.

A general result from the discussion in section 4.2 is the following: *A shear band with a chemical (i.e. bonding) energy associated to its interfaces forms by a discontinuous mechanism and not through a homogeneous process or the rigid propagation of an interface.* This applies to shear bands on all length scales from atomistic shear to macroscopic shear systems [28].

6.2. Type I and II twinning in 10 M Ni–Mn-Ga

For 10 M Ni–Mn-Ga and close to the martensite transformation temperature, the type I and type II twinning stresses are about 1.2 and 0.05 MPa [1]. Very close to the martensite/austenite equilibrium temperature, type I twinning stress can be as low as 0.3 MPa [35]. The twinning stresses increase linearly with decreasing temperature with −40 and −0.5 kPa/K [35,36]. In the following we discuss how the predictions of the present model correspond to these experimental results.

Table 1 lists the numerical values for the parameters needed for Equations ((14), (19), (21) and (22), and the sources providing these values or data supporting these values. Some of these values are not readily available and we discuss here our reasoning for the chosen figures.

Shear modulus: Ni–Mn-Ga is highly anisotropic with an extremely low C' modulus near the austenite/martensite phase transformation. Seiner et al. report that C' increases linearly with temperature in the austenite phase and assumes a value of 3.6 GPa at 380 K [37]. Linear extrapolation to the martensite transformation temperature of 219 K yields about 1.5 GPa for C'. Heczko et al. relate the low C' modulus to a high magnetoelastic coupling constant, which peaks at the transition temperature indicating that C' increases slowly with decreasing temperature in the martensite phase [38]. Chernenko et al. report a 3 GPa Young modulus for the martensite phase near the martensite transformation [39], which suggests an even smaller C' in the martensite phase near the martenstite/austenite equilibrium temperature. The Young modulus increases linearly with decreasing temperature. The very compliant elasticity of Ni–Mn-Ga near the martensite transformation agrees with complete softening of the TA_2 phonon branch in the austenite and martensite phases [40]. All these results are consistent with a C' modulus, which is almost zero just below the martensite transformation temperature (we choose $C' = 0.5$ GPa at the transition temperature) and increases slowly and linearly with decreasing temperature to a value of approximately 15 GPa at 0 K.

Step height, Burgers vector, twinning shear: These parameters vary with structure, lattice parameters, and, thus with composition. The variations are small, though, and unimportant in the scope of this study as discussed in section 2. We use parameters consistent with electron microscopy analyses of twinning disconnections [41,42].

The values listed in Table 1 yield values of 4.7 and 0.33 MPa for τ_{I} and τ_{II} at the martensite transformation temperature, which is in the right order of magnitude. For zero Kelvin, the model predicts 140 and 10 MPa. Experimental data for type I twinning is not available for such low temperatures. For type II twinning, 10 MPa is substantially higher than the 0.2 MPa deduced from magnetic switching field experiments [36]. The overestimation of the type II twinning stress at low temperature results from the neglected temperature dependence of the interface relaxation parameter α. This parameter represents the compliance of the lattice. Thus, as the shear modulus increases with decreasing temperature, α decreases accordingly. If we were to include the temperature dependence of α, the model predicted a lower twinning stress at low temperature.

For the activation energies we obtain $E_{\mathrm{AI}} = 0.13$ meV and $E_{\mathrm{AII}} = 0.1$ meV. This suggests that twinning is athermal to very low temperatures of about 2–3 K for both twinning types. This is in very good agreement with results from Straka et al. who measured the magnetic switching field for type II twins down to 1.7 K [36]. For a sample without intermartensitic transformation, the switching field increased linearly with decreasing temperature from room temperature to 1.7 K. These results confirm that type II twinning is athermal. At higher temperature, the twinning stress depends on temperature only through the temperature dependence of the shear modulus, of the interface relaxation parameter α, and of the twinning shear. The latter dependence is weak. For type I twinning, data is available for the temperature range down to 40 K below the martensite transformation temperature [35]. In this range, the type I twinning stress increases linearly with decreasing temperature indicating athermal twinning in agreement with our findings.

The transition from thickness growth (nascent disconnection loop) to lateral growth (at constant step height) occurs at h_{c}. This is the step height of type II twinning and it is about one order of magnitude smaller than the step height of type I twinning. Therefore, the type II twinning Burgers vector $\mathbf{b}_{\mathrm{II}}$ is about one order of magnitude smaller than the type I twinning Burgers vector $\mathbf{b}_{\mathrm{I}}$ and so are the associated stress fields. The elastic interaction force of crystal defects (interstitial atoms, impurities, small angle grain boundaries etc.) with dislocations is proportional to the dislocation stress field. Thus, the hardening effect of such impurities is substantially reduced for type II twins as compared to type I twins.

6.3. Dependence of type II twinning stress on R_{nII}

The type II twinning stress slowly decreases with increasing the nucleus radius R_{nII} (Equation (19)). Multiplying the radius with or dividing it by 2 decreases or increases the twinning shear stress by about 40%. The nucleus radius is not a material parameter. It

Table 1
Parameters for equations ((14), (19), (21) and (22); numerical values are given for 10 M Ni–Mn-Ga near the martensite transformation temperature.

Parameter, symbol, unit	Value	Source	Comment
Shear modulus, G, GPa	0.5	[36–40]	varies with temperature
Poisson ratio, ν, -	1/3		
Step height, h_{I}, Å	2	[41,42]	yields b_{I} with Eq. (2) for Eq. (14)
Inner dislocation cut-off radius, ρ, Å	1		of the order of an atomic radius
Breaking distance, r_0, Å	1	[14]	of the order of an atomic radius
Twinning shear, s, -	0.12	[41,42]	varies with lattice parameters
Loop radius, R_{nII}, Å	20		must be larger than 5ρ
Interface relaxation parameter, α, -	0.025	[14]	varies with shear modulus

depends on the local atomic arrangement and varies from position to position. We assume that the nucleus radius is equal to or larger than R_{cl} (Equation (13)) although by no more than about one order of magnitude. The reason for the upper limit is the positive and stronger than linear dependence of the activation energy on the nucleus radius (Equation (22)). From the experimental finding that type II twinning is not thermally activated at 1.7 K follows that the activation energy is less than about 0.2 meV and, thus, the nucleus radius must be less than about 10 nm.

Some authors describe the deformation-induced removal of twin boundaries in a shape memory alloys with the term "detwinning". Aside from twin nucleation, twinning (which includes twin nucleation) and detwinning (which excludes twin nucleation) are identical processes. Since we consider here only the propagation of a twin boundary which does not include twin nucleation, the results apply to twinning and detwinning alike. Nucleation of a twin requires a higher stress than twin boundary motion. Thus, for a single domain shape memory alloy single crystal, the initial twinning stress is higher than the stress required for continuous deformation as demonstrated by Aaltio et al. [43].

7. Conclusions

We presented a twinning model based on the disconnection structure of twin boundaries. From the elastic property of the interface followed the general result that twin boundaries move through the motion of twinning disconnections. We considered the homogeneous nucleation of disconnection loops. The first law of thermodynamics provided conditions for the twinning stresses for type I and type II twins. The twinning stress of type II twins is approximately fourteen times lower than that of type I twins. For type I twinning, the activation energy is a material constant whereas for type II twinning, the activation energy depends on structural fluctuations in the interface. At temperatures with thermal energy higher than the activation energy, the twinning stress depends on temperature only through the temperature dependences of the shear modulus and the lattice constants and in the case of type II twinning on the interface relaxation parameter α (which depends on the shear modulus). For 10 M Ni–Mn-Ga, thermal activation is significant only below about 3 K. Within the limits of isotropic linear elasticity, the model predicts twinning stresses for 10 M Ni–Mn-Ga reasonably well.

Acknowledgements

The author acknowledges financial support by the National Science Foundation through grant No. NSF-DMR-1710640.

References

[1] L. Straka, O. Heczko, H. Seiner, N. Lanska, J. Drahokoupil, A. Soroka, S. Fähler, H. Hänninen, A. Sozinov, Highly mobile twinned interface in 10 M modulated Ni-Mn-Ga martensite: analysis beyond the tetragonal approximation of lattice, Acta Mater. 59 (2011) 7450–7463.
[2] J.W. Christian, S. Mahajan, Deformation twinning, Prog. Mater. Sci. 39 (1995) 1–157.
[3] M.A. Meyers, A. Mishra, D.J. Benson, Mechanical properties of nanocrystalline materials, Prog. Mater. Sci. 51 (2006) 427–556.
[4] Y.T. Zhu, X.Z. Liao, X.L. Wu, Deformation twinning in nanocrystalline materials, Prog. Mater. Sci. 57 (2012) 1–62.
[5] R.J. Asaro, P. Krysl, B. Kad, Deformatoin mechanism transitions in nanoscale fcc metals, Phil. Mag. Lett. 83 (2003) 733–743.
[6] K. Otsuka, C.M. Wayman, Shape Memory Materials, Cambridge University Press, Cambridge UK, 1998.
[7] E.K. Salje, Phase Transitions in Ferroelastic and Co-elastic Crystals, Cambridge University Press, Cambridge, UK, 1993.
[8] K. Bhattacharya, G. Ravichandran, Ferroelectric perovskites for electromechanical actuation, Acta Mater. 51 (2003) 5941–5960.
[9] K.M. Rahman, V.A. Vorontsov, D. Dye, The effect of grain size on the twin initiation stress in a TWIP steel, Acta Mater. 89 (2015) 247–257.
[10] B.C. De Cooman, Y. Estrin, S.K. Kim, Twinning-induced plasticity (TWIP) steels, Acta Mater. 142 (2018) 283–362.
[11] L. Straka, N. Lanska, K. Ullakko, A. Sozinov, Twin microstructure dependent mechanical response in Ni-Mn-Ga single crystals, APL 96 (2010), 131903.
[12] M. Ahlers, The martensitic transformation: mechanisms and crystallography, Phil. Mag. 82/6 (2002) 1093–1114.
[13] L. Capolungo, I.J. Beyerlein, Nucleation and stability of twins in hcp metals, Phys. Rev. B 78 (2008), 024117.
[14] J. Wang, H. Sehitoglu, Twinning stress in shape memory alloys: theory and experiments, Acta Mater. 61 (2013) 679–6801.
[15] D. Kellis, A. Smith, K. Ullakko, P. Müllner, Oriented single crystals of Ni-Mn-Ga with very low switching field, J. Cryst. Growth 359 (2012) 64–68.
[16] A. Saren, T. Nicholls, J. Tellinen, K. Ullakko, Direct observation of fast-moving twin boundaries in magnetic shape memory alloy Ni-Mn-Ga 5 M martensite, Scripta Mater. 123 (2016) 9–12.
[17] A. Smith, J. Tellinen, K. Ullakko, Rapid actuation and response of Ni-Mn-Ga to magnetic-field-induced stress, Acta Mater. 80 (2014) 373–379.
[18] E. Faran, D. Shilo, Ferromagnetic shape memory alloys – challenges, applications, and experimental characterization, Exp. Tech. 40 (2016) 1005–1031.
[19] J.P. Hirth, R.C. Pond, Steps, dislocations and disconnections as interface defects relating to structure and phase transformations, Acta Mater. 44 (1996) 4749–4763.
[20] J.M. Howe, R.C. Pond, J.P. Hirth, The role of disconnections in phase transformations, Prog. Mater. Sci. 54 (2009) 792–838.
[21] K.V. Vladimirsky, On the twinning of calcite, Zh. Eksp. Teor. Fiz. 17 (1947) 530–536.
[22] F.C. Frank, J.H. van der Merwe, One-dimensional dislocations 1. Static theory, Proc. Roy. Soc. Lond. A 198 (1949) 205–216.
[23] R. Bullough, Deformation twinning in the diamond structure, Proc. Roy. Soc. Lond. A 241 (1957) 568–577.
[24] R.W. Cahn, Survey of recent progress in the field of deformation twinning, in: R.E. Reed-Hill, J.P. Hirth, H.C. Rogers (Eds.), Deformation Twinning, Gordon and Breach Sci. Publ., New York, 1964, pp. 1–28.
[25] J.P. Hirth, J. Lothe, Theory of Dislocations, second ed., Krieger Pub. Co., Floriday, 1982, p. 814.
[26] R.C. Pond, J.P. Hirth, Topological model of type II deformation twinning, Acta Mater. 151 (2018) 229–242.
[27] R.C. Pond, J.P. Hirth, K.M. Knowles, Topological model of type II deformation twinning in NiTi martensite, Phil. Mag. 99 (2019) 1619–1632.
[28] P. Müllner, Plastic deformation: shearing mountains atom by atom, J All. Comp. 577S (2013) S96–S101.
[29] P. Müllner, A.E. Romanov, Internal twinning in deformation twinning, Acta Mater. 48 (2000) 2323–2337.
[30] A.E. Romanov, V.I. Vladimirov, in: F.R.N. Nabarro (Ed.), Disclinations in Crystalline Solids, Dislocations in Solids, vol. 9, 1992, pp. 191–402.
[31] P. Müllner, A.H. King, Deformation of hierarchically twinned martensite, Acta Mater. 58 (2010) 5242–5261.
[32] J.P. Hirth, J. Lothe, Theory of Dislocations, second ed., Krieger Pub. Co., Floriday, 1982, p. 169.
[33] R.L. Fleischer, Substitutional solution hardening, Acta Metall. 11/3 (1963) 203–209.
[34] T. H. Courtney, Mechanical Behavior of Materials, second ed. Waveland Press, Inc. 2000, Long Grove, Illinois, pp. 186-196
[35] L. Straka, A. Soroka, H. Seiner, H. Hänninen, A. Sozinov, Temperature dependence of twinning stress of Type I and Type II twins in 10M modulated Ni-Mn-Ga martensite, Scripta Mater. 67 (2012) 25–28.
[36] L. Straka, A. Sozinov, J. Drahokoupil, V. Kopechý, H. Hänninen, O. Heczko, Effect of intermartensitic transformation on twinning stress in Ni-Mn-Ga 10 M martensite, J. Appl. Phys. 114 (2013), 063504.
[37] H. Seĩner, O. Heczko, P. Sedlák, L. Bodnárová, M. Novotný, J. Kopeček, M. Landa, Combined effect of structural softening and magneto-elastic coupling on elastic coefficients of Ni-Mn-Ga austenite, J. All. Comp. 577s (2013) S131–S135.
[38] O. Heczko, Magnetoelastic coupling in Ni-Mn-Ga magnetic shape memory alloy, Mater. Sci. Forum 635 (2010) 125–130.
[39] V. Chernenko, J. Pons, C. Seguí, E. Cesari, Premartensitic phenomena and other phase transformations in Ni-Mn-Ga alloys studied by dynamical mechanical analysis and electron diffraction, Acta Mater. 50 (2002) 53–60.
[40] S. Ener, T. Mehaddene, B. Pedersen, M. Leitner, J. Neuhaus, W. Petry, Vibrational properties of Ni-Mn-Ga shape memory alloy in the martensite phases, New J. Phys. 15 (2013), 123016.
[41] R.C. Pond, B. Muntifering, P. Müllner, Deformation twinning in Ni_2MnGa, Acta Mater. 60 (2012) 3976–3984.
[42] N. Zárubová, Y. Ge, J. Gemperlová, A. Gemperle, S.-P. Hannula, Funct. Dislocation mechanism of twinning in Ni-Mn-Ga, Mater. Lett. 5 (2012), 1250006.
[43] I. Aaltio, O. Söderberg, Y. Ge, S.-P. Hannula, Twin boundary nucleation and motion in Ni-Mn-Ga magnetic shape memory material with a low twinning stress, Scripta Mater. 62 (2010) 9–12.